Princeton Plasma Physics Laboratory

PPPL-5353

EC power management for NTM control in the ITER baseline scenario

F. M. Poli, E.D. Fredrickson, N. Bertelli

February 2017

Prepared for the U.S.Department of Energy under Contract DE-AC02-09CH11466.

Princeton Plasma Physics Laboratory
Report Disclaimers

Full Legal Disclaimer

Trademark Disclaimer

PPPL Report Availability

Princeton Plasma Physics Laboratory:

http://www.pppl.gov/techreports.cfm

Office of Scientific and Technical Information (OSTI):

http://www.osti.gov/scitech/

Related Links:

U.S. Department of Energy

U.S. Department of Energy Office of Science

U.S. Department of Energy Office of Fusion Energy Sciences

EC power management for NTM control in the ITER baseline scenario

F.M. Poli, E.D. Fredrickson, N. Bertelli

Princeton Plasma Physics Laboratory, Princeton, NJ. 08543, USA.

E-mail: fpoli@pppl.gov

M.A. Henderson, S-H Kim

ITER Organization, Route de Vinon-sur-Verdon, CS 90 046, 13067 St. Paul lez Durance Cedex. France

D. Farina, L. Figini

Istituto di Fisica del Plasma, Milano, Italy

E. Poli

Max-Planck-Institute for Plasma Physics, 85748 Garching, Germany

Abstract. Time-dependent simulations are used to evolve self-consistently plasma discharges in combination with a modified Rutherford equation for calculation of Neoclassical Tearing Mode (NTM) stability in response to Electron Cyclotron (EC) feedback control in ITER. The main application of this integrated approach is to support the development of control algorithms by analyzing the plasma response with physics-based models and to assess how uncertainties in the detection of the magnetic island and in the EC alignment affect the ability of the ITER EC system to fulfill its purpose. Simulations indicate that it is critical to detect the island as soon as possible, before its size exceeds the EC deposition width, and that maintaining alignment with the rational surface within half of the EC deposition width is needed for stabilization and suppression of the modes, especially in the case of modes with helicity $(2,1)$. A broadening of the deposition profile, for example due to wave scattering by turbulence fluctuations, can even be favorable in the case of the $(2,1)-$NTM, by relaxing the over-focussing of the EC beam and improving the stabilization at the mode onset. Pre-emptive control reduces the power needed for suppression and stabilization in the ITER baseline discharge to a maximum of 5 MW, which should be reserved and available to the Upper Launcher during the entire flattop phase. With pre-emptive control ITER would be still able to demonstrate a fusion gain above $Q = 9$.

Submitted to: *Nuclear Fusion*

1. Introduction

Among the external heating and current drive systems planned in ITER, the Electron Cyclotron system (EC) has the highest flexibility. In fact, by combining the equatorial and the upper launcher, the EC can cover up to 85% of the plasma cross-section, missing about 10% of the edge and about 5%-10% near the axis, allowing for combined central heating, current profile tailoring and MHD stability control of sawteeth and Neoclassical Tearing Modes [1, 2, 3].

Applications of the EC system include (a) breakdown and burn-thru assist in a limited plasma for flux consumption saving, (b) ramp-up assist and H-mode access (c) MHD control and central heating in the flattop phase (d) ramp-down assist and exit from H-mode and (e) plasma termination. Every application has to be accurately balanced with the other heating and current drive sources for optimization of HCD resources.
An important application of the EC system is NTM control and stabilization, for which the Upper Launcher (UL) has been specifically designed, to provide localized deposition down to 2% of the minor radius [1, 2, 3, 4, 5, 6]. The power is provided by 24 gyrotrons operating at a frequency of 170 GHz and power of 1 MW each, of which 0.83 MW are delivered to the plasma on account of transmission losses from the gyrotron diamond window to the plasma boundary. Figure 1 shows the layout of the UL, which comprises of four ports, each housing eight beam lines, arrayed in a upper and lower row of four

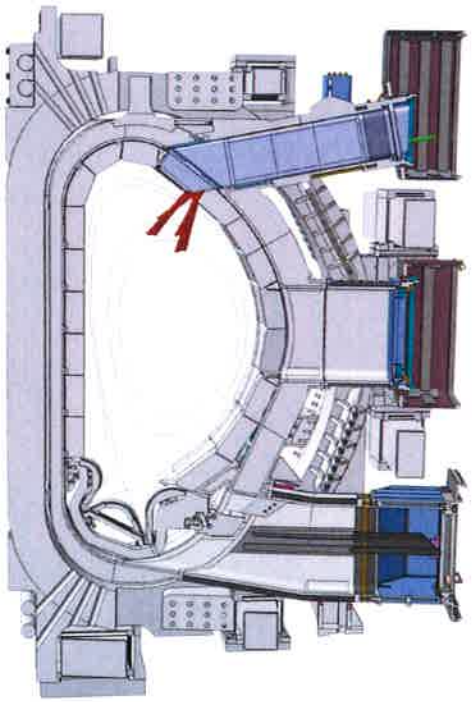

Figure 1. ITER plasma cross-section and structures, with the layout of the Upper Launcher and the beam aiming from the Upper Steering Mirror (USM) and the Lower Steering Mirror (LSM), aiming here respectively at the $q = 1.5$ and the $q = 2.0$ surface.

waveguides each, dubbed Upper Steering (USM) and Lower Steering (LSM) mirror. The UL can deliver the total 20MW of power, with up to two thirds on either steering mirror.

Localized current drive by radiofrequency waves, deposited inside a magnetic island, is an effective way of stabilizing nonlinear tearing modes, as shown in the pioneering work by A. Reiman, which explores the case of lower hybrid waves [7]. The most successful experimental application of rf waves for tearing mode stabilization has however been demonstrated with injection of EC waves, which can provide the necessary profile localization at the rational surfaces $q = 1.5$ and $q = 2$ (see, for example, the review by Maraschek [8]).

Assessment of the power needed for NTM control and stabilization in the ITER baseline are usually expressed in terms of the figure of merit $\eta_{NTM} \equiv j_{CD}/j_{BS}$, defined as the ratio of the EC current density to the bootstrap current density at the rational surface. Criteria for the value of η_{NTM} go back to the work by Hegna and Callen [9], who predicted for ITER $\eta_{NTM} = 1.5$, followed by Zohm [6] who predicted $\eta_{NTM} = 1.2$. The derivation of η_{NTM} has since been the subject of progressively more accurate derivations, which are surveyed in the review by E. Poli [10]. Recently, a more integrated approach has been adopted, where - instead of using time slice data or tabulated values - ray-tracing calculations and the evolution of the island rotation frequency and width with a Modified Rutherford Equation (MRE) were calculated offline from a baseline scenario developed with JINTRAC [11, 12]. However, those offline calculations did not account for modifications of the magnetic equilibrium and of the pressure profiles in response to the EC heating and current drive.

Herein we describe a different approach, more consistent, but yet not entirely self-consistent, where the MRE is solved during the simulation and a feedback control is used to steer the mirrors and to change the EC power level in response to the NTM stability. The main application of this integrated approach - which is the focus of this work - is to support the development of control algorithms and to assess the effect of uncertainties in the detection of the magnetic island and in the equilibrium reconstruction on the ability of the ITER EC system to fulfill its design requirements. A second, important application is scenario development and design of discharges that satisfy at the same time stability and performance, since one of the ITER goals is to demonstrate operation at fusion gain of $Q = 10$, where $Q = 5P_\alpha/P_{ext}$ is the ratio of the fusion power from self-heating alpha power P_α to the power from external sources P_{ext}.

The approach undertaken for the calculations in TRANSP [15] is described in Sec.2 and the MRE adopted here is summarized in the Appendix. Section 3 discusses the stability in the ITER baseline plasma, by comparing two simulations that differ only for 6% in the pedestal pressure, but sensibly in the plasma performance and in the NTM stability. Section 4.1 discusses the control and stabilization of modes that have grown above the critical size, while Sec.4.2-7 discuss pre-emptive control and how this is affected by the alignment between the EC deposition and the rational surfaces and by a broadening of the deposition profile. Finally, Sec.9 concludes with some remarks on the implications of these results on discharge design for performance and control, on the

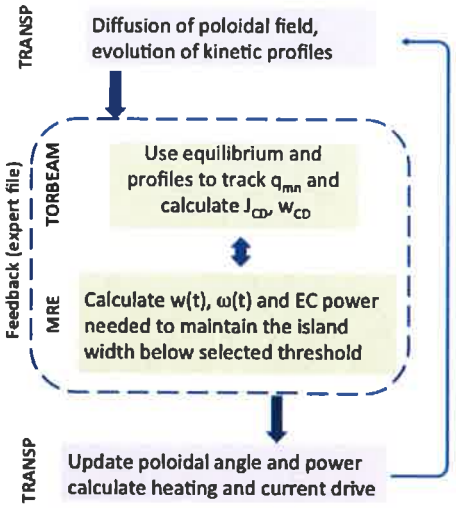

Figure 2. Schematics of the interface between TRANSP and the EC controller for NTM stabilization.

required accuracy in the EC alignment, as well as giving recommendations for further analysis and for research on control algorithms applied to ITER.

2. Calculation of NTM stability in TRANSP, with EC feedback control

In order to assess the EC control system requirements, it is important to simulate the evolution of the NTM island in combination with the plasma magnetic equilibrium and the kinetic profiles, as they evolve in response to the external heating and current drive. Approaches based on a modified form of the Rutherford Equation [13] are routinely used for calculations of NTM stability, as well as reduced models for real-time control oriented algorithm [14].

The TRANSP transport solver [15] has an unique capability of being used in conjunctions with so-called "expert files". Expert files are external coding that are linked to the main executable and that allow users to manipulate the simulations by including additional features. A direct application of expert files is for simulations dedicated to develop control algorithms and it has been applied on NSTX-U for control of the plasma performance [16, 17] and of plasma rotation [18] with Neutral Beam Injection. In this respect expert files can provide valuable inputs for control requirements, diagnostic sensitivity or combined actuator control development, because they allow to test the plasma response to external perturbations in the presence of high-fidelity physics models.

In order to provide a real-time simulated response of the plasma, a Modified Rutherford Equation (MRE) has been interfaced with TRANSP. The MRE used here is based on the approach by Fredrickson [19], which was validated against (3, 2)-NTMs on TFTR [20]. The approximations used in the calculation of the tearing stability have been shown to be accurate for magnetic islands with width up to 20% of the plasma

minor radius [19].

The contribution from the EC heating and current drive have been implemented to the original MRE using the formulation by Bertelli *et al* [35] and DeLazzari *et al* [49]. Details of the terms included into the MRE for the evolution of the island width are summarized in the Appendix and a schematics of the interface and of the EC feedback control is shown in Fig.2. The feedback control consists of two parts: one provides the evolution of the width and rotation frequency of the island and the other interfaces the calculation of the island stability with a feedback control on the poloidal steering mechanism and of the input power. The island frequency rotation is not discussed herein since all cases analyzed in this work, except for the unmitigated $(2,1)$-NTM with large pedestal pressure gradient shown in Fig.4-(g) do not lock.

The part that deals with the control of the EC power and steering uses the beam tracing code TORBEAM [21] and can be pre-programmed for combined applications, like sawtooth and NTM tracking and control. The interface between TRANSP and the MRE-based feedback control is implemented thru an expert file. The calculations in the expert file are done on the time step of the Heating and Current Drive sources, which is here $\Delta t = 5$s unless otherwise stated, while the MRE is evolved over time steps of 25 ms during Δt; for comparison, the energy confinement time in the ITER baseline scenario is [36] $\tau_E = 3.7HH \simeq 3-4$s, for a confinement gain HH close to unity, consistently with the simulations discussed herein. At each source time step t_1 the width and the frequency of the magnetic island are evolved between t_1 and $t_2 = t_1 + \Delta t$, using $40\Delta t$ time steps in the internal evolution of the MRE, under the assumption that the pressure profiles and the magnetic equilibrium are stationary over Δt. The time step of the feedback control and of the HCD source calculations is not limited to 5s, but it can be further reduced considering the mirror poloidal steering time-scale. It should be noted that the TRANSP/MRE interface in its present state does not include a reduction of the global confinement with the island width and this is our motivation for stating a lack of self-consistency in the approach presented herein. This reduction in confinement will be introduced when the MRE is implemented self-consistently in the TRANSP code, at which time the stability will be calculated over time scales comparable to the transport time scales.

3. NTM stability in the baseline scenario

Figure 3 shows two TRANSP simulations of the ITER 15MA ELMy H-mode, used as a reference in this work for the NTM analysis. The current ramp-up phase is 80s long, with the plasma being diverted at about 12s and the radio-frequency heating and current drive being turned-on shortly after. The electron density is built-up fast to $2 \times 10^{19}\mathrm{m}^{-3}$ within the first 20s to provide a background plasma for good absorption of both Electron and Ion Cyclotron waves. The EC power is turned-off in the flattop in both simulations, under the assumption that this power is needed for NTM stabilization. The electron density profile is prescribed in time, while the electron and ion temperature profiles

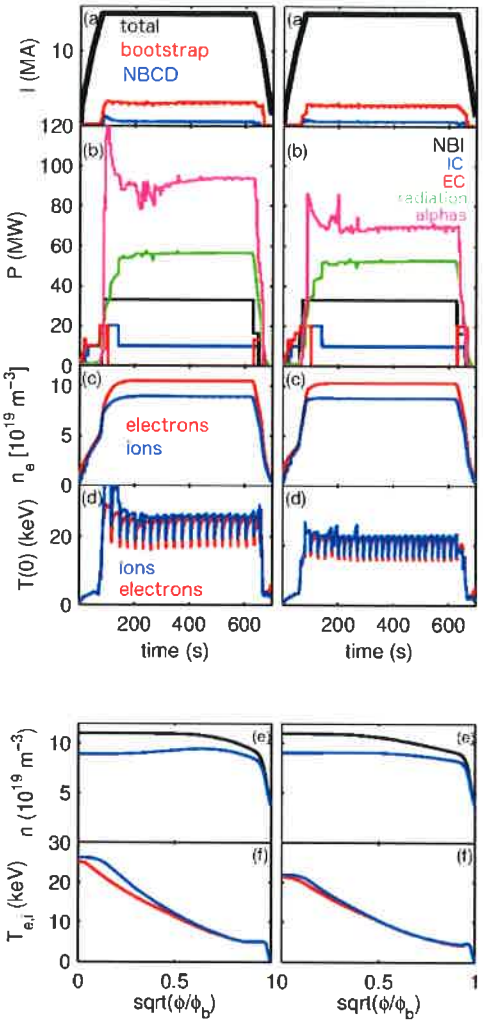

Figure 3. Time traces for the baseline scenario for two assumptions of the L-H transition time: at the end of the flattop phase (left) and at about three quarters of the ramp-up phase (right column). (a) plasma current, NB driven current and bootstrap current (b) injected external power, radiated power and α power. (c) line integrated density for electrons, ions and impurities, (d) electron and ion temperature, central value. (e) density profiles at 480s (f) temperature profiles at 480s.

are evolved using the GLF23 [22. 23] turbulence transport model. The pedestal width and height are interpolated from a lookup table constructed with the EPED1 peeling-ballooning stability model [24]. EPED1 uses input parameters such as pedestal density, shape parameters, the plasma composition Z_{eff} and the normalized magnetic to plasma pressure β_N to predict the pedestal width and height. There are 987 EPED1 calculations in the look-up table covering the range of parameters expected for the ITER baseline scenario [25]. Because the pedestal width and height are interpolated at each time step, the discharge evolution and the core profile evolution are nonlinearly related to the pedestal structure and vary during the simulation, responding to variations in β_N, shape

and Z_{eff}. The impurity profiles are the same as the electron density profile, rescaled according to a fraction that is prescribed in time; impurity fraction levels assumed here in the flattop phase are Berillium at 2% of the electron density, Argon 0.1% and Tungsten up to 10^{-5} of the electron density.
The two simulations differ in the time of entry to H-mode, which is 80s in the case shown in the left column and 65s in the case shown in the right column. The transition from L- to H-mode is set by increasing the level of injected power above the threshold power provided by the ITPA scaling [26] and by changing the density profile from a more peaked to a more flat profile with a pedestal. After the L-H transition the electron density rapidly builds-up to the flattop value of $0.85n_G$. Since entry to H-mode is imposed in both cases at half the Greenwald density n_G, the two cases are also using different density evolution during the last third of the current ramp-up phase. It should be noted that the average density rise during the L-H transition might be faster than assumed in these simulations and comparable to about five times the energy confinement time, *i.e.* about 15 seconds.

The large increase in the alpha power at the entry to burn is a consequence of using a prescribed density profile across the L-H transition and it is related to a similar transient increase in the pedestal temperature to satisfy the pedestal pressure calculated from the EPED1 lookup table. Self-consistent simulations should evolve all transport channels with a coupled core-edge plasma model, for an assessment of the conditions of entry to H-mode in response to the heating and current drive sources mix. Since the density profile is prescribed, the two selected cases are meant to show how uncertainties in the underlying assumptions can affect the conclusions on NTM stability and EC power assessment. With small differences in the density pedestal structure and in the L-H transition assumptions, the two simulations evolve to different operational points. The plasma with earlier H-mode access has a core temperature that is about 20% lower (6% lower pedestal temperature) in the flattop phase, which results in a drop of P_α of about 30% and of Q from 10.5 to 7 under the same assumptions of external input power P_{ext}.

Figure 4 compares the evolution of the bootstrap current at the rational surfaces of $q = 1.5$ and $q = 2.0$. The lower pedestal gradient results in a lower bootstrap current at the $q = 2$ surface and therefore to a lower amplitude of the neoclassical contribution to the $(2, 1)$-NTM. Since the density profiles are flat and the temperature profiles are rather stiff in the core, differences in the bootstrap current at the $q = 1.5$ surface are smaller. The two simulations have thus different neoclassical drive, which results in differences in the island width of about 20% at the $q = 1.5$ surface and about 50% at the $q = 2.0$ surface in the flattop phase. While earlier L-H transition results in an earlier appearance of the $(2, 1)$-NTM, the growth of both modes is slower, mostly due to the less steep rise of the bootstrap current at the respective rational surfaces.

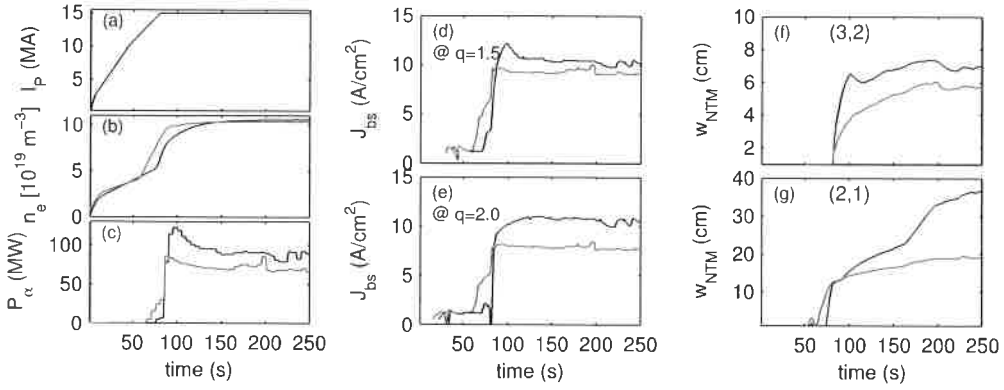

Figure 4. NTM stability for two different assumptions on the density evolution and the entry to H-mode. The red line refers to the early H-mode case, the black line to the late H-mode case. Left panel: (a) plasma current ramp-up (b) line averaged density (c) alpha particle self-heating power. Central panel: bootstrap current density for the same cases, calculated at (d) $q = 1.5$ and at (e) $q = 2.0$. Right panel: width of the NTM island calculated for the (f) $(3, 2)$ mode and for the (g) $(2, 1)$ mode.

3.1. Evolution of the NTMs in the baseline simulation

Figure 5 (top panel) shows the dominant contributions to the island width growth for the two plasma simulations in the flattop phase at 480s, as calculated by the MRE. The calculations are done for the $(m, n) = (3, 2)$ and $(2, 1)$ modes, in the absence of EC heating and current drive. Shown in the figure are the classical term $\Delta'(w)$ (blue), the contribution from the polarization current (magenta, Eq.5) which introduces a stabilization effect at small island width, the neoclassical contribution Δ'_{NC} (red shaded area, Eq.3) and the total growth rate Δ'_{tot} (black shaded area). The magnetic geometry contribution $\Delta'_{GGJ}(w)$ term (Eq.6) also introduces a stabilization for small island width and is included in the calculations, but not shown in Fig.5, being negligible compared to the others. The shaded area indicates the range of uncertainty in the results for two choices of the constant k_1 in the neoclassical contribution (see Eq.3), namely $k_1 = 0.20$ and $k_1 = 0.16$, which correspond respectively to the values of 3.2 and 2.6 used by Sauter [27] and derived in the case of large aspect ratio tokamaks [29, 30] and geometrical effects [32]. The coefficient in the contribution from the polarization current is instead maintained unity. Increasing this coefficient according to previous estimates for ITER [27] increases the seed island size by about 25%. However, this does not affect the main conclusions on our analysis on the levels of power needed, especially in the case of the $(2, 1)$-NTM, which is predicted here to grow from its seed size to a width comparable to the EC deposition width over time scales shorter than 3s.

There are two solutions for $\Delta'_{tot} = 0$, one at small width, which corresponds to the critical size w_{seed} (seed island) above which NTMs are triggered, and one at large island width, dubbed w_{sat} (saturated island) which corresponds to the stabilization of the magnetic island from the equilibrium current. The critical size is $w_{seed} = 1.5$ cm in

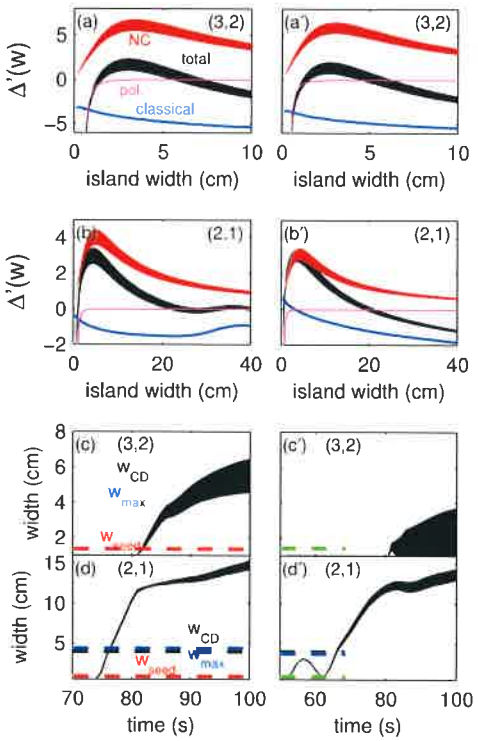

Figure 5. Top: Δ' terms for the $(3,2)$ and the $(2,1)$ modes, calculated at 480s; neoclassical contribution (red), classical tearing term (blue), small-island stabilization contribution from the polarization term Δ'_{pol} (magenta) and total contribution (black). The Δ'_{NC} term accounts for uncertainties in the value of k_1, which are reflected in the total growth rate. Bottom: time evolution of the width of the NTM island at $q = 1.5$ and $q = 2.0$; the colored area accounts for the variation due to the choice of k_1. The average flattop value of w_{max}, w_{seed} and w_{sat} and of the ECCD deposition with w_{CD} are shown for comparison.

the case of the $(3,2)$ mode and about 1 cm in the case of the $(2,1)$ mode, values much smaller than the resolution of the ECE diagnostic, which is estimated to be below 6 cm [33]. The magnitude of w_{seed} is also below the sensitivity of the magnetic equilibrium reconstruction, which is projected to be larger than 3 cm from reconstruction methods on JT-60U and on DIII-D [34]. The width corresponding to the maximum growth rate Δ'_{max} is $w_{max} \simeq 4$ cm for both modes. The value of w_{max} is the reference target for NTM stabilization and for the calculations of η_{NTM} from the condition $dw/dt = 0$ [10, 35]. Techniques for NTM control should aim at dropping the value of Δ'_{max} to zero and maintaining the size of the island below w_{max} [34].

The value of w_{sat} is about 5-7 cm in the case of the $(3,2)$ for both plasma simulations, while it varies between 20 and 40 cm for the $(2,1)$-NTM depending on k_1 and on the pressure pedestal height. The pressure profile flattening inside the island leads to a relative degradation of the confinement τ_E, which can be estimated as [36]:

$$\frac{\Delta\tau_E}{\tau_E} = 4\rho_s^3 \frac{w_{sat}}{a} \qquad (1)$$

where ρ_s is the value of normalized minor radius where the NTM appears. The confinement degradation would increase from 5% in the case of a $(3,2)$-NTM at $\rho_s \simeq 0.65$ and with $w_{sat} \simeq 7$cm, to about 30% for a $(2,1)$-NTM at $\rho_s \simeq 0.80$ and with $w_{sat} \simeq 30$cm. It should be noted that w_{sat} for the $(2,1)$-NTM is sensitive to details of the pressure profiles and - in particular - to the pedestal pressure gradient. Differences in the values obtained here and those previously reported [36] are to be attributed mostly to the different pressure profiles and plasma current profiles used.

The features at large island width are an effect of calculating the tearing stability term from an integration of the current profile over the tearing layer rather than using a reduced, parametrized model. When the island width achieves large values, hitting the location of the pedestal, the large amplitude in the bootstrap current causes the $\Delta'(w)$ term to deviate from monotonic. This change in slope of the classical term is not observed in the plasma discharge with lower pedestal pressure.

Figure 5(c-d) shows the evolution of the islands at $q = 1.5$ and $q = 2.0$ at the first time the NTM appears, soon after entry to H-mode. There is a delay of about five seconds between the appearance of the $(2,1)$ and of the $(3,2)$ mode in the simulation with higher pedestal pressure and of about fifteen seconds in the simulation with lower pedestal pressure. The entry to H-mode is perhaps the most challenging phase for NTM control: depending on the density build-up rate compared to the plasma current ramp rate and how the heating and current drive sources are used to access H-mode, the poloidal flux surfaces might not have reached a stationary state, challenging the tracking of the rational surfaces where NTMs are most likely to be triggered. In addition, if the $(2,1)$-NTM is not controlled soon after its appearance, there is risk for a drop in the stored energy and a H-mode back transition. In this event, there could be a critical configuration in which the EC has to prevent NTM generation to occur to maintain the H-mode.

The stabilization at the $q = 2.0$ surface is challenged by the fast growth of the mode to a width comparable to the EC deposition w_{CD}, which is less than two seconds in the case with higher pedestal pressure and about fifteen seconds in the plasma with lower pedestal pressure. The average value of the typical island width and the deposition width of the ECCD in the current flattop phase are shown for comparison. The latter is calculated as the full width at half maximum of the current density profile, which is assumed to be a gaussian profile. While in the case of the $(3,2)$-NTM w_{CD} is larger than both w_{max} and w_{seed}, in the case of the $(2,1)$-NTM w_{CD} is comparable to w_{max}. The former situation is comparable to the conditions found on present-day tokamaks. It has been suggested that - under conditions where the EC deposition width is wider than w_{max} - modulation of the EC power is the preferable option for NTM stabilization [10, 35, 36]. The latter situation is instead atypical for present-day experiments, which challenges the ability of demonstrating the control of the $(2,1)$-NTM under conditions relevant to ITER in existing tokamaks. The EC system on ITER is designed for power modulation up to 5 kHz. Modulation is not considered in the simulations presented herein because the time window where $w_{CD} > w_{NTM}$ is too short and applies only to

the initial phase of evolution of the NTM, especially in the case of the $(2,1)$ mode. Power modulation might still be desirable during the early phases of evolution of the NTM, soon after its triggering. However, as it will be discussed in Sec.4.2, at these early stages of growth misalignment of the EC deposition is also more likely and the benefits of modulating the power might be canceled by depositing the power close to the X-point, thus further contributing to destabilization.

The range of uncertainty in the width of the $(3,2)$-NTM is large and simulations predict this mode to change between stable or unstable depending on the assumptions on the density profile evolution, the assumption on the calibrating coefficient k_1 and the pedestal pressure gradient. It should be noted that the switch mechanism that diverts the power between mirrors has an upper limit in the response time of 3 seconds. The combination of a small seed island, large detection threshold, narrow deposition width and fast growth rate suggest that there might be no sufficient time on ITER for active detection and stabilization of the $(2,1)$-NTM. Assuming that the control system reacts as soon as the island reaches 4 cm and that the power needed for stabilization is made available to the Upper Launcher within the limits of the hardware time scales, the island would have reached about 7-8 cm by the time the EC power is deposited to the $q = 2.0$ surface. This is the case for both assumptions on the ramp-up evolution. It will be shown in the following section that, assuming an uncertainty in the EC alignment comparable to w_{CD}, this is the minimum island width that can be maintained independently of the control scheme.

4. NTM control and stabilization

Approaches to NTM control can be divided into two categories: control of modes that have grown above the detection threshold size and prevention of the triggering of instabilities. The techniques most widely used in present-day tokamaks and the main results until 2012 are reviewed by Maraschek [8]. Subsequent to the publication of this review, progress has been made in the search and suppression of NTMs and in pre-emotive control on DIII-D [37, 38, 39], TCV [40, 41, 42, 43] and ASDEX-U [44, 45]. This section describes simulations where the input power is adjusted in response to the measured NTM width and growth rate (Sec.4.1) and where a constant amount of power is maintained on each rational surface for pre-emptive control (Sec.4.2). It is shown that the requested power is significantly lower in the case of pre-emptive control, provided a good alignment of the EC deposition with the rational surface is maintained.

4.1. Stabilization and suppression of an evolved island

This section discusses simulations with feedback control, where the EC input power is changed in response to the NTM width in order to either suppress the NTM or to reduce its width below a threshold value w_{min}. The time step for the EC calculations used here is $\Delta t = 3$s, which corresponds to the limit imposed by the switch that redirects the power

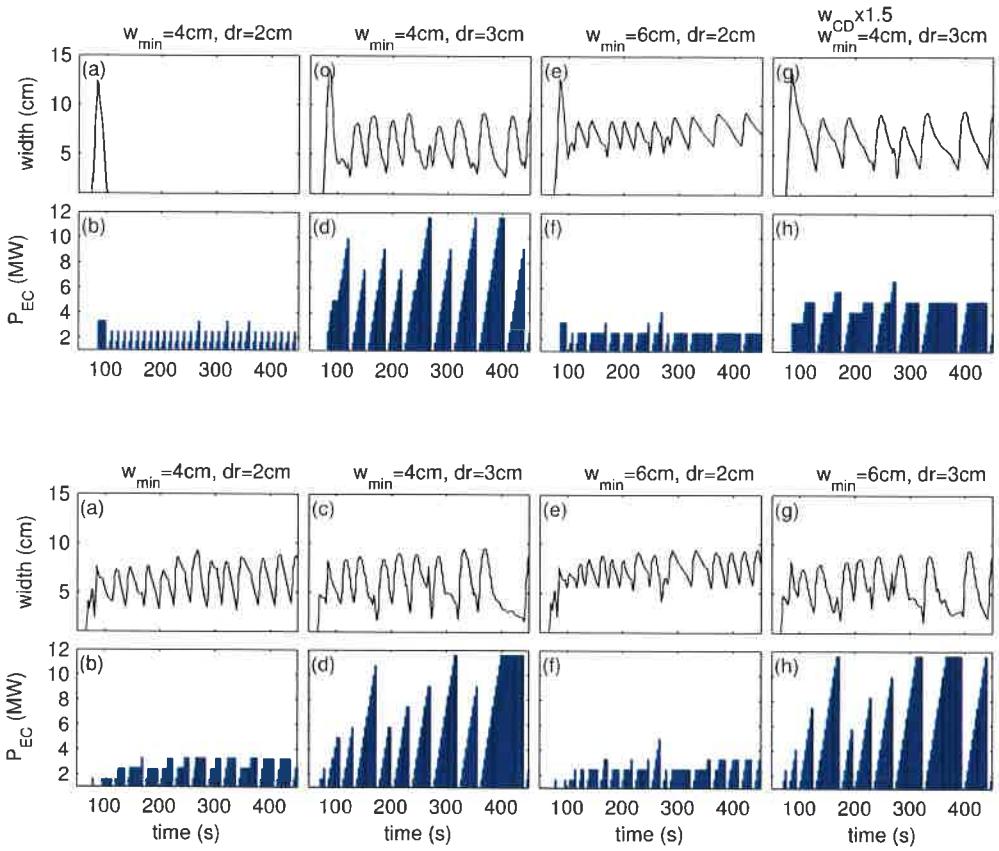

Figure 6. Results from TRANSP/MRE simulations in the case of the (2, 1) mode, where the EC input power is changed in response to the NTM island width and growth rate, for the plasma simulation with higher pedestal pressure and for the plasma simulation with lower pedestal pressure (bottom panel). For each case the NTM island width and the input EC power are shown. The cases shown make different assumptions on the detection threshold and on the distance between the EC deposition and the rational surface $q = 2$, $dr = |r_{CD} - r_q|$. In the case of high pedestal pressure, one case is shown where the EC deposition width has been increased by 50%.

from one mirror to another. For example, if the EC power is directed to the Equatorial Launcher for core heating and current profile tailoring and an NTM is detected, then three seconds are needed for the power to be available on the Upper Launcher. The time step used in the simulations mimics such delay in the response of the system.

We interpret here the calculated width and Δ'_{max} as proxies for the detection of the NTM from the ECE diagnostics and from the magnetic measurements. At each EC calculation time step the island width is evolved between t_1 and t_2, using the input power at t_1 and assuming that the pressure profiles and the magnetic equilibrium do not change between t_1 and $t_2 = t_1 + 3$s. If the island width has shrunk below w_{min}, and if $\Lambda'_{max} \leq 0$, then the input power is dropped to zero. This case corresponds to a fully suppressed island. If $\Delta'_{max} > 0$ and the island width is above the threshold size, the MRE calculates how much power is needed to reduce Δ'_{max} to zero and feedbacks this

power level to TRANSP. If $\Delta'_{max} < 0$ and $w > w_{min}$ the EC input power is maintained at a constant level. After the L-H transition and each time the EC power is turned-off after NTM suppression, the EC power is turned-on only when the island width grows above w_{min}. Two values of w_{min} are considered here, equal to 4cm and 6cm based on the upper limit on the ECE resolution [33] and the projected lower limit on the magnetic equilibrium reconstruction [34].

Figure 6 shows the results for the two reference plasma simulations discussed in the previous section. The final operational point is different from the cases shown in Fig.3 because of the use of ECCD that modify the current and temperature profile and the fusion gain. For completeness an assessment on the effect of the distance between the location of the EC deposition r_{CD} and the rational surface r_q. $dr = |r_{CD} - r_q|$ is included in the calculations. An upper limit of 13.4 MW is set on the power that can be delivered to the LSM, which is tracking the $q = 2$ surface. Consequently, the upper limit on the power that can be delivered to the USM. which is tracking the $q = 1.5$ surface, is 6.67 MW. Interestingly, in both plasmas the maximum requested power is comparable under the same assumptions on w_{min} and on dr, because the maximum width reached by the island is well below w_{sat} of 20-40 cm for the (2, 1)-NTM and the early stages of evolution from w_{seed} to w_{min} are the same. This suggests that early control and stabilization is critical. We also notice that the maximum power depends on the value of $|r_{CD} - r_q|$ more than the value of w_{min}; thus up to 4 MW is required if $dr \simeq 2$cm for both values of w_{min}. This is important, because it indicates that alignment between the EC deposition location and the rational surfaces is a more stringent requirement than increasing the signal to noise ratio in the detection threshold of diagnostics dedicated to the detection of NTMs down to values comparable to w_{CD}.

Another observation is that the NTM promptly grows back shortly after the EC power has been removed from the rational surface, because of the large neoclassical drive. These simulations are assuming a 'sea' of islands with width just below the critical size w_{seed}, ready to be triggered at the appearance of any perturbation. This is not an unrealistic assumption, since the large β_N on ITER would make NTM metastable and susceptible of being triggered not only from sawtooth crashes, as observed in present-day, low-β_N experiments, but also from other external or internal disturbances, like ELMs and pellets [27]. The expected frequency of unmitigated ELMs on ITER is about 1-2 Hz [46], which would trigger about two NTMs every second. Although ITER will operate with mitigation schemes that are expected to increase the ELM frequency up to 30-60 Hz and to reduce their amplitude [46], it is not unreasonable to assume - as it is done here - that NTMs can be triggered anytime.

Thus a question arises whether pre-emptive control of NTMs via destabilization of long period sawteeth might be sufficient condition for NTM pre-emption on ITER. Although this control approach has been highly successful in present-day experiments using ECCD [41, 43], the high β_N and the meta-stable NTM condition in ITER may require a most robust and effective NTM pre-emption scheme. The broad deposition profile of the upper Launcher at the $q = 1$ surface, in particular, would limit its

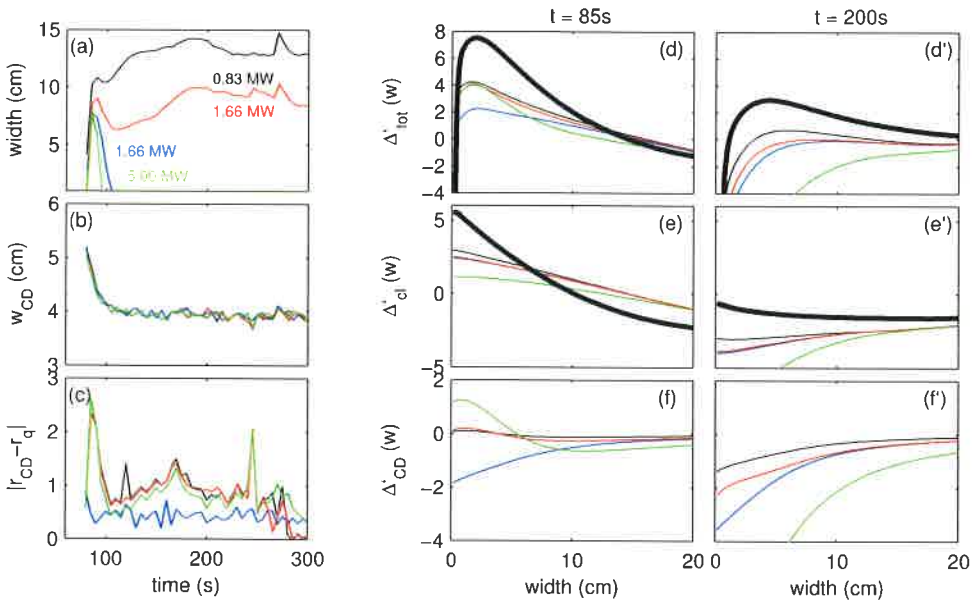

Figure 7. TRANSP/MRE simulations in the case of the $(2,1)$ mode for a scan of the input EC power. Left panel: (a) island width (b) ECCD deposition width, (c) distance between the EC deposition center and the rational surface. The blue and red curve use the same input EC power level, but the tolerance for alignment is more conservative in the blue case. Middle and right panels: (d) Δ'_{tot}, (d) Δ'_{cl}, (e) Δ'_{CD} for the same cases shown in the left panel, at two different time steps. The contributions to Δ' for the unmitigated case are shown for comparison as thick black curves.

applicability to modify locally the magnetic shear for sawtooth triggering and implies that a search for an integrated control using various actuators that can access the $q = 1$ surface would be highly desired. Alternate approaches to pre-emptive control have been explored on AUG, where a $(4,3)$-NTM is triggered to prevent either the $(3,2)$ or the $(2,1)$ from appearing [8]. The feasibility of this solution on ITER is worth consideration, especially if this method can be proven to be beneficial for the pre-emption of the $(2,1)$-NTM. However, because the MRE used in our simulations does not treats the interaction between magnetic islands, the discussion is not included in this analysis.

The frequent on/off of the EC system that is calculated by the EC feedback control and that is triggered by the fast growth of the $(2,1)$-NTM suggests that maintaining a constant, low level of power on the $q = 2$ surface after NTM suppression is recommended for pre-emption as opposed to actively searching for the mode to be detected or wait until its width exceeds the detection threshold. An implication is that this power should be reserved and available to the Upper Launcher all time, at the expenses of other applications, for example core heating and bulk current drive. For this reason, it is imperative to optimize the discharge for MHD stability and the diagnostics accuracy for alignment in order to minimize the amount of power that is needed for NTM stabilization. Pre-emptive control does minimize these power requirements.

4.2. Pre-emptive NTM control and power requirements

The simulations discussed in the previous section indicate that the NTM grows back as soon as the EC power is removed from the rational surface, suggesting that pre-emptive control might be a preferable approach in ITER, by maintaining a constant power on each rational surface and minimizing redirection of power between launchers and turning on/off the gyrotrons. This section discusses simulations where a fixed amount of power is maintained on each rational surface starting from the entry to H-mode, which is when NTMs first appear. The amount of power is changed from the minimum available, which is 0.83 MW (one gyrotron) to the maximum available power to each steering mirror, which is either 6.67 MW or 13.4 MW.

The results are shown in Fig.7. The tracking algorithm has been pre-programmed to allow for a maximum misalignment of 0.5 cm, which is far below the resolution of the magnetic equilibrium reconstruction. We dub this case (blue curve) the 'perfect alignment' that is used for comparison with the other simulations. Only the $(2,1)$-NTM is discussed here, since the $(3,2)$-NTM is predicted to be stable with minimum applied power, if the ECCD is well aligned with the $q = 1.5$ surface. Similarly to what found in the previous section, these simulations conclude that maintaining a good alignment with the rational surfaces is important, and that a large $dr = |r_{CD} - r_q|$ at the onset on the NTM affects the time and the power needed for full suppression. The blue and red curves assume the same input power of 1.66 MW, but they have different d. While the $(2,1)$-NTM is fully suppressed shortly after trigger in the case with prefect alignment (blue curve), its width is reduced to about 10 cm when $d \simeq 1$ cm (red curve). This case corresponds to stabilization, as indicated in Fig.7-d' by the reduction of Δ_{max} down to zero. Increasing the input power to 5 MW would suppress the mode in about 10s (green curve). One may ask whether assuming $dr \simeq 1$ cm is an acceptable assumption or still technically challenging even in this pre-emptive control case. This will be addressed in the next section.

The early stages of evolution of the NTM are particularly critical for stabilization and control, as shown in the central column, where the classical and ECCD contribution to the total Δ'_{tot} are shown. The curves corresponding to the case without ECCD are shown for comparison (thick black). The deposition of ECCD close to the rational surface modifies the current profile and reduces the magnitude of Δ'_{cl} at all stages of evolution, by an amount that increases with the input power. However, this contribution is destabilizing in early H-mode for all values of $w < w_{sat}$. At 85s, *i.e.* shortly after the NTM is triggered above w_{seed}, the Δ'_{CD} is always stabilizing only in the case of perfect alignment (blue curve) and destabilizing until the island grows to a size comparable to the deposition width w_{CD} when $dr > 0.5 w_{CD}$. These cases correspond to a situation where the ECCD is driven close to the island X-point. For widths $w > w_{CD}$ the contribution of Δ'_{CD} is always stabilizing since the EC deposits the current inside the island. We also point out that the parametrization of the misalignment effect $G(w)$ is valid only for $w \leq w_{CD}$ [49]. The plasma simulation with lower pedestal pressure

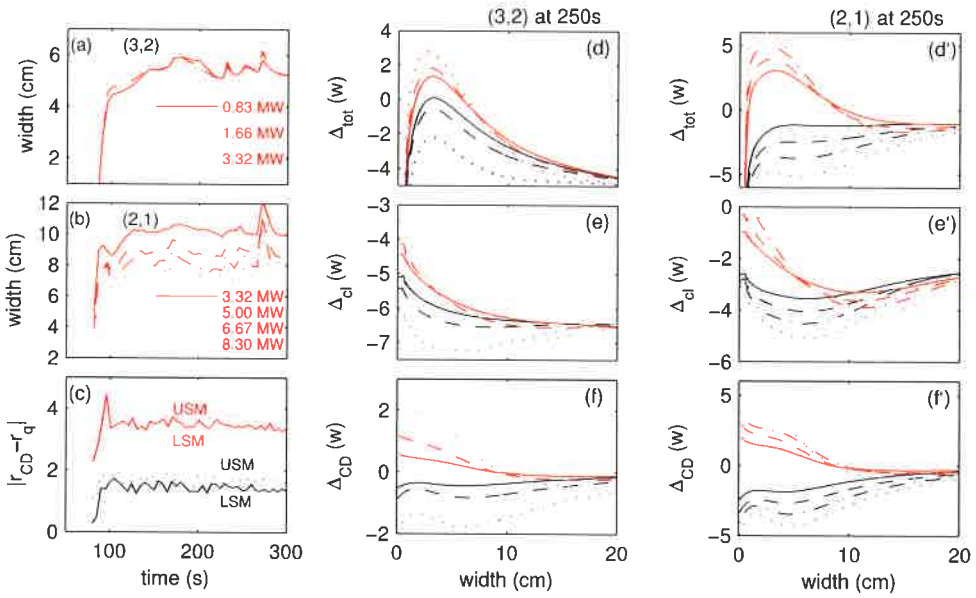

Figure 8. TRANSP/MRE simulations for a scan of the distance $dr = |r_{CD} - r_q|$ between the ECCD deposition and the rational surface for fixed input EC power of 1.66MW on the USM (aiming at $q = 1.5$) and 3.32MW on the LSM (aiming at $q = 2.0$). Left panel: (a) island width of the $(3, 2)$ mode (b) island width of the $(2, 1)$ mode, (c) distance between the EC deposition center and the rational surface. Middle and right panels: (d-d') Δ'_{tot}, (e-e') Δ'_{cl}, (f-f') Δ'_{CD} for the $(3, 2)$ and the $(2, 1)$ mode, calculated at $t = 90$s. TRANSP/GRE simulations in the case of the $(2, 1)$ mode for a scan of the input EC power. Left panel: (a) island width (b) ECCD deposition width, (c) distance between the EC deposition center and the rational surface. Middle and right panels: (d) Δ'_{tot}, (d) Δ'_{cl}, (e) Δ'_{CD} for the same cases shown in the left panel, at two different time steps.

is predicted to be stable against NTMs with pre-emptive application of the minimum available power for comparable values of $dr \simeq 1$cm and it is not shown here. In the next section it is shown that relaxing the tolerance on dr increases the requirements on the maximum power needed for stabilization.

5. Effect of misalignment on the stabilization and suppression

The effect of a loss of alignment between the EC deposition location and the rational surfaces where NTMs are triggered has been analyzed by other authors [10, 48, 49]. The conclusion from previous analysis was that maintaining alignment within $0.5w_{CD}$ is critical [48]. The time-dependent simulations discussed here confirm these results. Moreover, they highlight that the most critical phase is the triggering of the mode and that even a moderate misalignment at the NTM onset can affect the stabilization at later stages.

To complete the discussion started in the previous section, Figs. 8-9 show simulations where the maximum tolerance on the misalignment is increased above 1cm

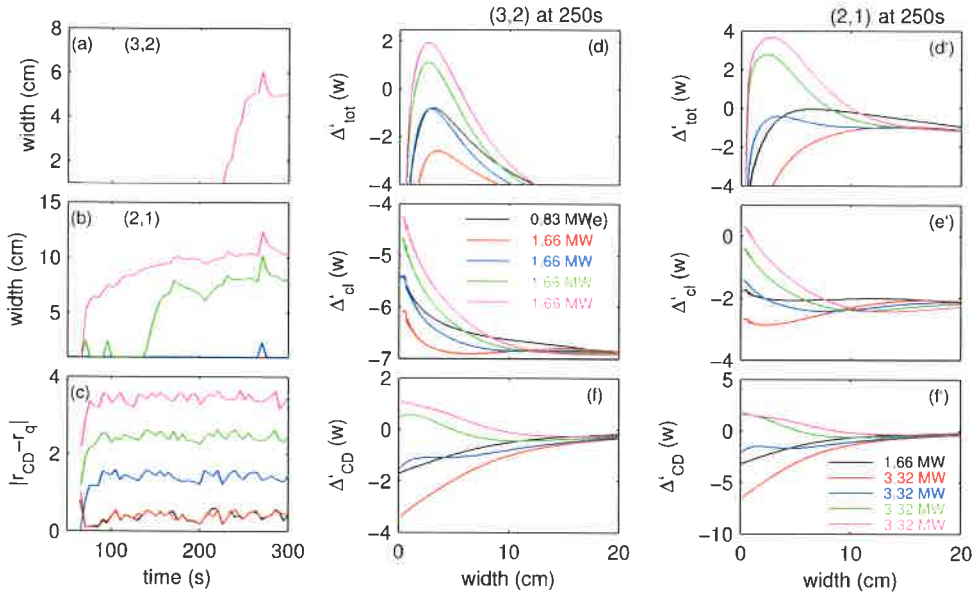

Figure 9. Same as Fig.8, but for the case with lower pedestal pressure and earlier L-H transition. In this case only two values of power are assumed on both rational surfaces.

during the entire flattop phase, for the two plasmas with higher and lower pedestal pressure respectively. It is assumed a constant level of input power on both rational surfaces, which - in the case of the plasma with higher pedestal pressure - is equal to one, two and four gyrotrons on the $q = 1.5$ surface, and four, six, eight and ten gyrotrons on the $q = 2.0$ surface.

In both plasmas maintaining $dr \leq 2$cm is a necessary condition for NTM suppression, which is achieved with 0.83 MW in the case of the $(3, 2)$-NTM and with 3.32 MW in the case of the $(2, 1)$-NTM in the plasma with higher pedestal; it is achieved with 0.83 MW at both rational surfaces in the plasma with lower pedestal pressure. When the tolerance on the alignment is increased up to 4cm, the width of the $(3, 2)$-NTM cannot be reduced below 6cm even with larger amount of power. With reference to Figs.4-5 this is comparable to the size of an unmitigated NTM. Since the energy confinement reduction caused by an unmitigated $(3, 2)$-NTM with $w_{sat} = 7$cm would be about 5%, and the reduction in Q for a mitigated NTM with 3.32 MW of injected power would be about twice as large, the decision whether to control this mode or not depends on the consequences that it has on the global stability of the plasma.

The width of the $(2, 1)$-NTM is moderately sensitive to the injected power and decreases from about 10cm to 7cm when the power is increased from 3.32MW to 8.3MW, although there is limited advantage in increasing the power above 6.67MW. This reduction in size corresponds to a reduction of a factor four from the unmitigated case and it is sufficient to avoid mode locking of the $(2, 1)$-NTMs. Also in this case, the decision on what control scheme is a compromise between the reduction in plasma

confinement and fusion gain and the maximum size of the magnetic island the plasma can survive without risking a disruption.

The results in the case of the plasma with lower pedestal pressure and neoclassical drive, shown in Fig.9. are qualitatively similar. The minimum width that can be maintained increases with increasing dr. A difference with the previous case is that both the $(3,2)$-NTM and the $(2,1)$-NTM are triggered at later times with improving the alignment. This is a consequence of the slower growth rate of the NTMs in this plasma and it suggests that with adequate discharge design and control of the global plasma parameters the growth rate of NTMs can be reduced with tangible advantages for NTM control. Because of the different approach used here and the consistent evolution of the magnetic equilibrium and the pressure profiles in response to feedback or to pre-emptive control, the power needed for full stabilization obtained here are more optimistic than values found in previous analysis that includes the effect of incorrect alignment of the EC on the NTM stability [48, 49. 50].

Thus, independent of the global plasma parameters and the conditions of entry to H-mode, with an initial injection of up to 10 MW of power at the L-H transition, when the $(2,1)$-NTM is more likely to be triggered, for a duration of about 10 seconds as found in Sec.4.1, the NTM could be stabilized or suppressed. Then, with a minimum amount of power, let's say 1.66 to 3.32 MW, injected continuously during the flattop phase, the size of the NTM can be maintained at a constant value of about 10 cm, sufficiently small to avoid mode locking [34, 48]. During this phase of sustainment the EC would deposit entirely inside the island and a correct alignment is no longer an issue.

6. On the importance of calculating NTM stability self-consistently with the plasma evolution

The magnetic equilibrium and the pressure profile evolve nonlinearly in response to the EC heating and current drive and therefore the NTM stability at each time step is affected by the plasma parameters at the previous time step. It is important that these nonlinearities are taken into account when assessing the power needed for stabilization, because this strongly depends on the plasma conditions as they evolve in time. Figure 10 shows calculations of the MRE offline, on the plasma simulation with higher pedestal pressure. The EC input power and the driven current in the Δ'_{CD} have been varied between 0.83 MW and 6.67MW assuming that the $J_{CD,max}$ term scales linearly with the power and that the EC deposition is aligned with the $q = 1.5$ and the $q = 2.0$ rational surfaces. The reference values for the deposition width and $J_{CD,max}$ have been taken from one of the simulations with minimum power discussed in the previous section. For completeness, the calculations have been repeated by assuming a fixed distance between the EC current deposition peak location and each rational surface.

The power scan indicates that - in the case of perfect alignment - the $(3,2)$-NTM would be fully suppressed with 0.83MW, after less than 20s from its triggering. When $dr = 2$cm, even the maximum power available to the USM would be insufficient to

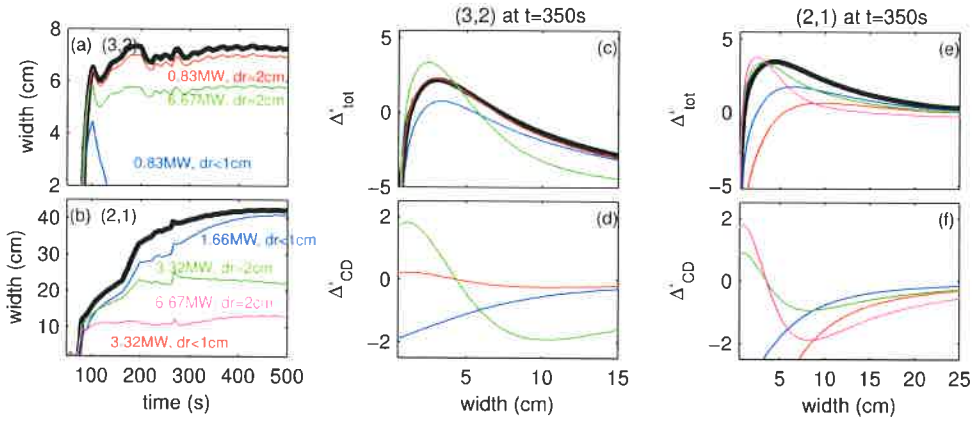

Figure 10. Offline MRE calculations. Left: evolution of the NTM width for different assumptions on the input EC power and the distance $|r_{CD} - r_q|$. Center: Δ' in the case of the $(3,2)$: (c) Δ'_{tot} and (d) Δ'_{CD}, same assumptions as in (a). Right panel: Δ' in the case of the $(2,1)$; (e) Δ'_{tot} and (d) Δ'_{CD}, same assumptions as in (b)

suppress the mode. The offline calculations are qualitatively similar for the $(2,1)$-NTM and indicate full suppression with perfect alignment and reduction of the width to 10cm with 6.67 MW. The results are qualitatively similar to the cases shown in the previous sections, namely the mode can be fully suppressed with a low amount of power in the case of perfect alignment. They are more pessimistic when the tolerance on dr is relaxed. In this case the $(2,1)$-NTM is predicted to be stabilized to about 10 cm and the $(3,2)$-NTM to about 6cm with maximum available power for $dr \simeq 2$ compared to $dr \simeq 4$ found in the previous section. We notice that these more pessimistic results are closer to previous projections for ITER [48, 35, 49, 50] and are most likely a consequence of not having included in those calculations the time-dependent response of the plasma to the ECCD.

7. Effect of broadening of the deposition profile

Excessive focussing of the USM on the $(2,1)$ surface might be a problem, especially when the EC deposition is not aligned with the rational surfaces, because it causes further destabilization of the island in its early stages of evolution, when its growth rate is largest. A logic conclusion is that a broader deposition profile would reduce the destabilizing effect of $dr > 0$ at the NTM triggering by enlarging the region that is covered by the ECCD.

It should be noted that the simulations discussed here are assuming a perfectly gaussian deposition profile [21], while in reality the EC profile is the superposition on individual beamlets from individual waveguides. This means that the modeled ideal focusing of the beam on the $q = 2.0$ surface, which was identified here as the main limitation for control, can be relaxed with appropriate pre-selection of the launchers and waveguides. Another mechanism for broadening occurs naturally in the plasma,

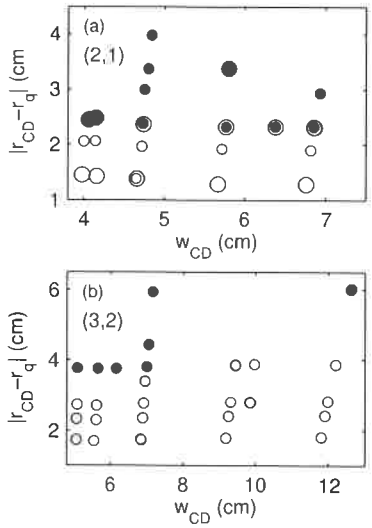

Figure 11. Results of TRANSP/MRE simulations for a scan over the ECCD deposition width and the average distance between the ECCD deposition and the rational surfaces. (a) Results for the $(2,1)$ mode. Empty symbols indicate full suppression, solid symbols can indicate either stabilized or unstable NTMs. Small symbols indicate discharges where the EC input power is 3.32MW, larger symbols indicate input power of 5MW. (b) Results for the $(3,2)$ mode. The EC input power is 1.16MW in all cases. Solid symbols indicate unstable discharges.

because of the presence of turbulence fluctuations that scatter the EC waves. Waves are scattered in random directions and on average the rays will follow the original trajectory calculated in the absence of fluctuations. The average effect will be a broadening of the deposition profile and a consequent reduction of the maximum current drive peak, which has been deemed responsible for an increase of the requested power for stabilization [10]. The final deposition profile is the combination of the two effects, which are modeled here by increasing the initial beam waist. This correction to the initial launching conditions modifies the broadening of w_{CD} at the resonance location; the corresponding value of $J_{CD,max}$ will be reduced accordingly to the beam tracing calculations. As opposed to rescaling the magnitude of w_{CD} and $J_{CD,max}$ that enter directly in the Δ'_{CD} contribution to Eq.2, this approach accounts for the effect of the ECCD on modifying the pressure profile and of the magnetic equilibrium self-consistently.

Figure 11 shows results from simulations that scan the deposition width w_{CD} and the value of dr. For each simulation the average value of the NTM island width in the flattop is calculated; values below w_{seed} correspond to suppressed NTMs and are indicated with open symbols, while values above w_{seed} are unsuppressed NTMs (they might be stabilized) and are indicated with solid symbols. The EC input power on the $q = 1.5$ surface is 1.66 MW, while two levels of power are considered on the $q = 2.0$ surface, namely 3.32 MW (smaller symbols) and 5.0 MW (larger symbols). On both rational surfaces a separation is observed between stable and unstable simulations that depends on dr. The $(3,2)$-NTM can be suppressed for $dr < 3$ cm, while the $(2,1)$-NTM

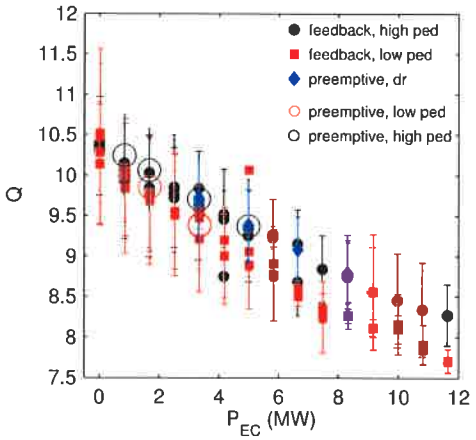

Figure 12. Variation of the fusion gain Q with the power deposited on the $q = 2$ surface. Solid symbols indicate simulations with active control in the case of high pedestal pressure (solid black) and of the low pedestal pressure (solid red), open symbols indicate simulations with preemptive control and perfect alignment for the high (black) and low (red) pedestal pressure, blue symbols indicate all the other cases with pre-emptive control and scan over dr.

is suppressed for $dr < 2$cm, *i.e.* for values of dr smaller than the nominal deposition width w_{CD}. These results are consistent with those discussed in the previous section.

Interestingly, the suppression of the $(3, 2)$-NTM is achieved increasing the broadening at constant power and $dr \simeq 4$cm. This seems in contradiction with previous reported analysis [10] that increasing the broadening would increase the power needs. In reality this is the consequence of reducing the destabilizing effect of a not perfectly aligned ECCD in the early stages of evolution, since the NTM island would grow entirely in the region covered by the ECCD. As shown in Fig.7-b, w_{CD} is wider at the end of the ramp-up phase before relaxing to stationary flattop values and this effect is further amplified by a broadening of the deposition width, either artificial or due to turbulence fluctuations. Since the TRANSP-MRE calculations account for the evolution of the plasma parameters in time, improving the stability at earlier stages has a positive impact on the NTM stability at later stages. This further stresses the advantages of pre-emptive control compared to the search of an already developed NTM.
The case of the $(2, 1)$-NTM is qualitatively similar. A moderate broadening of the deposition profile from 4 to 5 cm would favor NTM suppression with an increase of the input power from 3.32 MW to 5 MW for $dr > 2$cm, but less than 3cm. The EC system can achieve this by distributing the power over multiple launchers and spreading the deposition of the beams by using different mirrors.

8. How NTM control affects plasma performance

NTMs cause a degradation of the confinement that can be recovered with suppression and/or stabilization with ECCD. However, increasing the input power will reduce the

fusion gain. Figure 12 summarizes the simulations presented in this paper with a focus on the variation of Q with the input power deposited on the $q = 2$ surface, following a similar approach previously taken by Sauter and based on analytical dependencies [36]. For each simulation the value of Q is averaged over all time steps that have the same input power, with error bars representing the standard deviation from the averaged value; different symbols are used for different control schemes and assumptions. The solid black circles represent the simulations with active feedback and dynamic adjustment of the input power in the case of high pedestal pressure, while the solid red squares represent the equivalent cases for the cases with low pedestal pressure, discussed in Sec.4.1. Simulations with pre-emptive control and perfect alignment, discussed in Sec.4.2, are indicated with open circles, black for the high pedestal and red for the low pedestal cases. The solid blue symbols represent all the other cases with pre-emptive control and $dr \geq 1$cm, discussed in Sec.5 and Sec.7. All these simulations are using constant IC power of 10 MW in the flattop phase.

As shown in the figure, when feedback control is used the value of Q can decrease from 10 to 7.5 in time windows where the EC power is maximum. On the other hand, when pre-emptive control is assumed, Q remains above 9 provided $dr \simeq 0.5\Delta_{CD}$. If an upper limit on the power needed for pre-emptive control of both the $(3, 2)$ and the $(2, 1)$ NTM is set to 6.67 MW, then the remaining 13.4 MW can be used for core heating and current profile tailoring. This would reduce the fusion gain further, unless the IC power is replaced by the EC power. The effect of the relative amount of IC and EC power on the discharge performance and on the sawtooth stability is beyond the scope of this paper and will be the subject of future work. The strategy for controlling (or non controlling) NTMs relies on a balance between demonstrating $Q = 10$ and maintaining a stable plasma while preventing disruptions. Thus, for example, a width of up to 6 cm for an uncontrolled $(3, 2)$-NTM and up to 10 cm for the $(2, 1)$-NTM with pre-emptive injection of 3.32 MW continuously are probably a good compromise to ensure stability, sustain fusion gain and keep large enough EC power available for the other applications.

9. Conclusions

Assessment of the power needed for NTM stabilization is one of the critical area of the research in support of ITER. Calculations are commonly done using modified representations of the Rutherford equation. The main difference between the analysis discussed here and previous assessment is that in this work the NTM stability is calculated by taking into account the plasma response to the EC feedback control, by evolving the magnetic equilibrium, current and pressure profiles and the island width at the same time. This approach highlights new aspects important for NTM control on ITER and different from typical situations observed in present-day experiments.

First, the large neoclassical drive and β_N on ITER make NTMs metastable and susceptible of being triggered by any external or internal perturbation; this, suppressed NTMs can be triggered soon after the EC power is removed from the respective rational

surfaces. This implies that it is recommended to maintain a pre-emptive, continuous level of power on the rational surface rather than actively searching for the mode. While this is a successful approach on present-day experiments [37, 38], it might not be applicable on ITER because of the small size of the seed island and because of the fast growth rate, in particular the (2, 1)-NTM.

Second, alignment of the EC deposition location with the respective rational surfaces is critical. This is no surprise and it has been stressed by other authors [10, 48, 49]. Alignment depends on diagnostics, on the accuracy of the magnetic equilibrium reconstruction, on the accuracy of the EC system alignment itself and on defocussing effects from turbulence. Similar to previous analysis [48], we also find that $dr = |r_{CD} - r_q| \simeq 0.5 w_{CD}$ is the maximum deviation from a perfect alignment that is tolerated for the success of NTM control. The accuracy of the magnetic equilibrium reconstruction projects to 3 cm and larger on ITER from the techniques used today [34]. Research in this area, on data reduction and analysis techniques to improve the accuracy down to 2 cm would be beneficial for the success of ITER.

When the effect of uncertainty in the alignment of the ECCD is taken into account, an upper limit for the stabilization of the $(2, 1)$ and of the $(3, 2)$-NTM is 5 MW for $dr \simeq 0.5 w_{CD} \simeq 2$cm and increases to 13.4 MW for $dr \simeq w_{CD} \simeq 4$cm in the case of a fully developed NTM. In either case the width of the $(2, 1)$-NTM would be about 10 cm. Pre-emptive control would require between one third to half of this power to sustain an island of the same size, making this approach essential to maintain a minimum power investment.

The main difference with previous results is that time-dependent simulations identify a need for earlier stabilization of the NTMs, especially the (2, 1) mode. If the NTMs are suppressed as soon as they are triggered, then a minimum amount of power is sufficient to maintain the stability of the plasma in flattop. An island 10cm wide can be sustained at the $q = 2$ surface with 1.66 to 5 MW of power, injected continuously.

While turbulence fluctuations reduce the current drive efficiency and increase the needed power for stabilization of an already developed NTM, they can actually be beneficial in the case of pre-emptive control. The broadening of the deposition profile which is caused by wave scattering may in fact reduce the destabilizing effect of a non-perfect alignment at the mode onset, by enclosing the NTM growth inside the region covered by the EC deposition. This effect can be further amplified by pre-selecting the waveguides and launchers aiming at the $q = 2$ surface. This is another argument in favor of pre-emptive control as opposed to an active search and detection.

Research on NTM stabilization and development of complex control algorithms is very active and highly successful on present-day experiments. However, projection of these techniques to ITER operation requires an additional step beyond projections based on these results. The use of time-dependent simulations that combine the plasma evolution with schemes for feedback control can represent in this regard a valuable tool for design of robust control algorithms on ITER, by testing these schemes with hardware constraints and high fidelity physics models.

Acknowledgments

We thank O. Sauter, S. Nowak and the colleagues at PPPL, F4E and IO who have contributed to the development of this work with suggestions and feedback. This work is supported by ITER contract IO/RFQ/13/9550/JTR and by DOE contract DEAC02-09CH11466. The views and opinions expressed herein do not necessarily reflect those of the ITER Organization.

10. Appendix

The equations for the evolution of the island width w interfaced with TRANSP are based on the work by E. Fredrickson [19], to which two terms for the ECCD and for the ECH have been added:

$$\frac{dw}{dt} = 1.22\frac{\eta}{\mu_0}\left[\Delta'(w) + \Delta'_{NC} + \Delta'_{pol} + \Delta'_{GGJ} + \Delta'_{ECCD} + \Delta'_{ECH}\right] \tag{2}$$

where μ_0 the magnetic permeability and η the neoclassical plasma resistivity, which is calculated in TRANSP using the NCLASS libraries [31].
The terms on the right hand side are summarized below. for an extensive description of how they have been derived the reader is referred to the original references. The $\Delta'(w)$ represents the drive or damping on the tearing mode imposed by the external solution. In TRANSP a quasi-cylindrical approximation is made, so that the $J_0(r)$ and $q(r)$ are not related by the simple cylindrical approximation, but they are integrated from the toroidal magnetic equilibrium code [19]. This approach gets the rational surfaces in the right location and maintains the equilibrium current $J_0(r)$ and the derivative $J'_0(r)$ terms consistent [19].

The second term on the right hand side represents the destabilizing effect of the bootstrap current J_{BS} and is given by [29]:

$$\Delta'_{NC} = k_1 \frac{16 J_{BS}}{s\langle J\rangle}\frac{w}{w^2 + w_d^2} \tag{3}$$

where

$$w_d = 5.1 k_d \frac{r_s}{\sqrt{\epsilon s n}}\left(\frac{\chi_\perp}{\chi_\parallel}\right)^{1/4} \tag{4}$$

measures the extent to which the cross-field transport can support a parallel temperature or density gradient [29]. Here s is the magnetic shear, r_s the radius of the rational surface, ϵ the local aspect ratio and k_1 and k_d two calibration coefficients. The correction to the w^{-1} dependence accounts for the existence of a threshold for instability of the tearing modes. The coefficient k_1 accounts for the fact that the derivation of the neoclassical term is not exact.

The third term on the right hand side is the polarization term [30]:

$$\Delta'_{pol} = -k_2 \frac{\rho_{\vartheta i}^2 \beta_{pol} g}{w^3}\left(\frac{L_q}{L_p}\right)^2 \tag{5}$$

Here $L_{q,p}$ represent the local gradient scale length of the q and pressure profile respectively, β_{pol} is the plasma poloidal beta, $\rho_{th,i}$ the ion poloidal gyroradius and the parameter $g \simeq \epsilon^{3/2}$ and it approaches unity in the limit of low collisionality [19]. The polarization term is important for small island sizes and it becomes a small contribution in the case of large island sizes.

The fourth term on the right hand side is the Glasser-Green-Johnson term [51]:

$$\Delta'_{GGJ} \approx -5.4 k_4 \frac{\beta_{pol}\epsilon^2 L_q^2}{r_s w |L_p|}\frac{q^2 - 1}{q^2} \tag{6}$$

The form used here is the derivation by Houlberg [31].

Finally, the last term is the stabilizing contribution of the localized EC current drive. There are several expressions for this term. The one used here is from Bertelli *et al* [35]:.

$$\Delta'_{CD} = k_6 16\pi^{1/2} \frac{\mu_0 L_q}{B_p} \frac{J_{CD,max}}{w_{CD}} F(\tilde{w}) M(\tilde{w}, D) G(\tilde{w}, x_{dep}) \tag{7}$$

with [35]

$$F(\tilde{w}) = 0.25 \frac{1 + 0.96\tilde{w}}{1 + \tilde{w}(1.5 + \tilde{w}(0.43 + 0.64\tilde{w}))} \tag{8}$$

where $\tilde{w} = w/w_{CD}$ is the island width normalized to the EC deposition width. The term $M(w)$ represents the effect of modulation [35]. In the cases discussed herein no power modulation is assumed and $M(w) = 1.0$. The term $G(w)$ represents the effect of misalignment of the EC deposition with the resonant surface. This term is important for the studies presented herein. The expression used in TRANSP uses the derivation in De Lazzari et al [49]:

$$G(w) = 1 - 2\frac{x_{dep}}{g(\tilde{w})}\, e^{-\left(\frac{x_{dep}}{g(\tilde{w})}\right)^2} \int_0^{x_{dep}/g(\tilde{w})} dt\; e^{t^2} \tag{9}$$

with

$$g(\tilde{w}) = \frac{0.38\tilde{w}^2 + 0.26\tilde{w} + 0.5}{\tilde{w} + 1} \tag{10}$$

where $x_{dep} = (r_{dep} - r_s)/w_{dep}$ represents the deposition location relative to the resonant radius, normalized to the EC deposition width. We note that there is a typo in Eq.15 of Ref.[49], although the figures in that paper have been derived using the correct formulation. This term is important for the studies undertaken herein, which aim at assessing the effects of systematic misalignments or the effect of transient misalignments, like those caused by a sawtooth crash. The effect of the EC heating is included in the MRE using the formulation of Bertelli et al [35], with the effect of misalignment $G(\tilde{w})$ from De Lazzari et al [49, 50]. This term is not discussed here, bacause it contributes for less than a fraction of a percent compared to the current drive contribution under ITER conditions. However, it can be significant in present day tokamaks, as demonstrated on TEXTOR [52].

[1] Henderson M.A., Saibene G., Darbos G., *et al* 2015 Phys. Plasmas **22** 021808
[2] Farina D., Henderson M.A., Figini L., and Saibene G., 2014 Phys. Plasmas **21** 061504
[3] Farina D., Henderson M.A., Figini L., Ramponi G. and Saibene G., 2012 Nucl. Fusion **52** 033005
[4] Henderson M.A., Chavan R., Bertizolo R. *et al*, 2008 Fusion Sci. Techn. **53** 139
[5] Ramponi G., Farina D., Henderson M.A., Poli E., Saibene G. and Zohm H., 2007 Fusion Sci. Techn. **52** 193
[6] Zohm H. *et al*, 2007 Plasma Phys. Control. Fusion **49** B341
[7] Reiman A.H., 1983 Phys. Plasmas **26** 1338
[8] Maraschek M., 2012 Nucl. Fusion **52** 074007
[9] Hegna C. and J. Callen, 1997 Phys. Plasmas **4** 2940
[10] Poli E. *et al*, 2015 Nucl. Fusion **55** 013023
[11] Nowak S., 2014 Fusion for Energy, internal report number $F4E\_D\_22P4BW - 01D0201$
[12] Nowak S., 2015 Fusion for Energy, internal report
[13] Rutherford P.H., 1973 Phys. Fluids **16** 1903
[14] W. Wehner and E. Schuster, 2012 Nucl. Fusion **52**, 074003.
[15] HAWRYLUK, R., An Empirical Approach To Tokamak Transport, in COPPI, B., editor, Physics of Plasmas Close to Thermonuclear Conditions: Proceedings of the Course Held in Varenna, Italy, 27 August-8 September 1979, volume 1, pp. 1946, Varenna, Italy, 1981, Elsevier Ltd. Website: `http://w3.pppl.gov/transp`
[16] Boyer M. *et al*, 2015 Nucl. Fusion **55** 053033
[17] Boyer M. *et al*, 2016, IAEA-FEC contribution, submitted to Nucl. Fusion
[18] Goumiri I. *et al*, 2016 Nucl. Fusion **56** 036023
[19] E. Fredrickson, M. Bell, R. V. Budny and E. Synakowski, Phys. Plasmas **7** 4112 (2000)
[20] Chang Z. *et al*, 1998 Phys. Plasmas **5** 1076
[21] Poli E., *et al* 2001 Comput. Phys. Commun. **136** 90
[22] Waltz R.E. *et al*, 1997 Phys. Plasmas, **4** 2481.
[23] Kinsey J.E. *et al* 2003 Fusion Sci. and Tech. **44** 763.
[24] Snyder P.B. *et al*, 2011 Nucl. Fusion **51** 103016
[25] Poli F.M. *et al*. *Implementation of reduced pedestal models in time-dependent simulations*, submitted to Plasma Phys. Controll. Fusion, February 2017.
[26] Martin Y.R. *et al* (2008) journal of Physics: Conf. Series **123** 012033
[27] Sauter O. *et al*, 1997 Phys. Plasma **4** 1654
[28] Houlberg W A *et al* (1997) Phys. Plasmas **4** 3230
[29] Fitzpatrick, 1995 Phys. Plasmas **2** 825
[30] Wilson H. *et al* 1996 Phys. Plasmas **3** 248
[31] Houlberg W. *et al*, (1997) Phys. Plasmas **4** 3230
[32] Chang Z. *et al*, 1995 Phys. Rev. Lett. **74** 4663
[33] Taylor G. *et al*, (2015) EPJ Web of Conferences **87** 03002
[34] La Haye R.J. *et al*, 2006 Nucl. Fusion **46** 451
[35] N. Bertelli, D. De Lazzari and E. Westerhof, Nuclear Fusion **51**, 103007 (2011)
[36] Sauter O. *et al*, 2010 Plasma Phys. Control. Fusion **52** 025002
[37] Kolemen E. *et al*, 2013 Fusion Engineering and Design **88** 2757
[38] Kolemen E. *et al*, 2014 Nucl. Fusion **54** 073020
[39] Welander *et al*, 2015 proceedings of the IEEE 26th Symposium on Fusion Engineering (SOFE), page 1-5
[40] Felici F. *et al* 2012 EPJ Web of Conferences **32** 020 05
[41] Felici F. *et al*, 2013 Nucl. Fusion **53**, 113018
[42] Canal G.P. *et al*, 2013 Nucl.Fusion **53** 113026
[43] Kim D. *et al*, 2014 Phys. Plasmas **21** 10.1063/1.4884349
[44] Rapson C *et al*, 2014 Fusion Engineering and Design **89** 568
[45] Stober J. 2015 EPJ Web of Conferences **87** 02017

[46] Loarte A. *et al*, 2014 Nucl. Fusion, **54** 033007
[47] Sauter O., 2004 Phys. Plasmas **11** 4808
[48] La Haye R.J. *et al*, 2008 Nucl. Fusion **48** 054004
[49] De Lazzari D. *et al*, 2009 Nucl. Fusion **49** 075002
[50] De Lazzari D. *et al*, 2010 Nucl. Fusion **50** 079201
[51] Gorelenkov N. *et al*, 1996 Phys. Plasmas **3** 3379
[52] Westerhof E. *et al*, (2007) Nucl. Fusion **47** 85

PPPL PRINCETON PLASMA PHYSICS LABORATORY

Princeton Plasma Physics Laboratory
Office of Reports and Publications

Managed by
Princeton University

under contract with the
U.S. Department of Energy
(DE-AC02-09CH11466)

P.O. Box 451, Princeton, NJ 08543
Phone: 609-243-2245
Fax: 609-243-2751

E-mail: publications@pppl.gov

Website: http://www.pppl.gov